



Article

Investigation of the Evolution of Stratum Fracture during the Cavity Expansion of Underground Coal Gasification

Zhen Dong ^{1,†} , Haiyang Yi ^{2,*} , Yufeng Zhao ^{1,†}, Xinggong Wang ³, Tingxiang Chu ², Junjie Xue ¹, Hanqi Wu ⁴, Shanshan Chen ¹, Mengyuan Zhang ¹ and Hao Chen ¹

¹ Research Institute of Petroleum Exploration & Development, PetroChina, Beijing 100083, China

² North China Institute of Science and Technology, Langfang 065201, China

³ Research Institute of Petroleum Exploration & Development, PetroChina Tuha Oilfield Company, Hami 839009, China

⁴ PetroChina Gas Storage Company, Beijing 100101, China

* Correspondence: haiyangyi@ncist.edu.cn

† These authors contributed equally to this work.

Abstract: The evolution of fracture zone controls the safety of underground coal gasification (UCG) in terms of gas emission and water leakage. In order to understand the fracture propagation in the confining rock of a UCG cavity with various influence factors, this paper implemented a set of numerical models based on different geological and operating conditions. Analysis was implemented on the mechanism of fracture propagation and its evolution characteristics, suggesting that (a) continuum expansion of the cavity leads a near-field fracture circle in confining rock initially, followed by the roof caving and successive propagation of shear band. (b) The key observed influence factors of fracture propagation are the grade of confining rock, overburden pressure, dimension of the cavity and gasifying pressure, the linear relationships between them, and the fracture height. Additionally, the fracture depth in the base board was mainly caused by tensile fracture. (c) A model was proposed based on the evolution of fracture height and depth in roof and base board, respectively. Validation of this model associated with orthogonal tests suggests a good capacity for predicting fracture distribution. This paper has significance in guiding the design of the gasifying operation and safety assessment of UCG cavities.

Keywords: underground coal gasification; fracture evolution; cavity expansion; safety assessment; gas emission; water leakage



Citation: Dong, Z.; Yi, H.; Zhao, Y.; Wang, X.; Chu, T.; Xue, J.; Wu, H.; Chen, S.; Zhang, M.; Chen, H. Investigation of the Evolution of Stratum Fracture during the Cavity Expansion of Underground Coal Gasification. *Energies* **2022**, *15*, 7373. <https://doi.org/10.3390/en15197373>

Academic Editors: Gang Lei, Weiwei Zhu, Zhenhua Wei and Liangliang Zhang

Received: 15 September 2022

Accepted: 3 October 2022

Published: 7 October 2022

Publisher's Note: MDPI stays neutral with regard to jurisdictional claims in published maps and institutional affiliations.



Copyright: © 2022 by the authors. Licensee MDPI, Basel, Switzerland. This article is an open access article distributed under the terms and conditions of the Creative Commons Attribution (CC BY) license (<https://creativecommons.org/licenses/by/4.0/>).

1. Introduction

Underground coal gasification (UCG) is an advanced method of clean coal utilization by chemical mining, which is characterized by good safety, less investment, high economic performance, etc. [1]. Despite the great efforts that have been devoted into this aspect, in terms of laboratory investigation and engineering practice, large-scale implementation of commercial production is still limited by certain reasons, including uncertain safety issues, environmental pollution, guaranteed equipment, etc. [2]. Among such reasons, fracture propagation in the confining rock of a cavity is a serious concern that requires controlling the safety of gas production [3–5].

Due to the high combustion pressure of coal during UCG, the confining rock of a UCG cavity is under the coupling effect of earth stress, thermal expansion, and gasifying pressure. Evidence from laboratory and numerical modelling suggests that continuum expansion of UCG cavities induce stratum movement, thereby leading to ground settlement, gas leakage, cavity sealing, etc. [6,7]. Therefore, researcher's interests have been aroused in terms of the mechanical characteristics, permeability performance, and fracture propagation of the confining rock under the high temperature and stress field. For instance, from the view of cavity expansion, Luo and Wang [8], Akbarzadeh and Chalaturnyk [9], Janoszek et al. [10]

investigated the confining rock during coal combustion, suggesting obvious changes in the mechanical properties of rock at high temperature and pore pressure. The permeability of near-field rock of a UCG cavity, as announced by Otto and Kempka [11], Wałowski [12], Madiutomo et al. [13], Ding et al. [14], experiences significant change during cavity expansion, while that of far-field rock is influenced to a limited degree. Meng et al. [5], Duan et al. [15], Jin et al. [16] investigated the fracture characteristics, evolution law and influence tendency induced by pore pressure, thermal damage, etc. All these works convince us that the fracture networks in the confining rock of a UCG cavity is developed during the cavity combustion. Especially, comparison between the UCG and normal coal mining made by [17,18] suggests that the speed of fracture propagation during UCG is faster than that under normal mining condition and these fracture networks provide a channel for gas leakage and water infiltration. Škvareková et al. [19] noted that gas or tar leakage from the cavity to subsurface is one of the main risks during UCG operation. During such leakage, the fracture network in the roof rock contributes the majority of the effort by fluid channel [13,20–22]. Therefore, the fracture network in the confining rock of UCG poses a threaten to the environmental safety and the UCG production.

In the terms of assessing the safety of UCG cavities with consideration to fracture networks, determination of the fracture zone is a difficult issue that needs to be solved. Recently, Li et al. [23] established a controlling equation with consideration to thermal–mechanical coupling action. According to numerical modelling, the fracture evolution of the overlying rock during UCG was investigated and it was found that a wide damage area was formed during the cavity expansion. Qin [24] distinguished the difference of water diversion fissures of coal mining and UCG and found that a “butterfly”-shaped fractured zone was formed in the UCG confining rock, while that of coal mining is approximately in the shape of an arch, and the height of fracture zone in UCG is approximately three times of that in coal mining. Lu et al. [25] studied the crack evolution of overlying rock according to physical and numerical modelling and the fracture zone exhibited a typical “three-zone” structure similar to that of coal mining. Lin [26] analysed the pilot test of UCG in Inner Mongolia, China, and the height of the water conduction fracture reached 65 m, that is, the possible height of the aquifer. Consequently, the corresponding UCG cavity was possibly subjected to a water hazard. Liu [27] studied the stability of roof layers of a UCG cavity based on multiphysical modelling, and the stress distribution in the roof rock layers was observed to be changeable due to high temperature, and a larger roof movement was measured than that of coal mining. Falshtynskyi et al. [28] investigated the substantiating parameters of the formation of stratification cavities in the roof rocks, and a model was developed to calculate the volumes of cavities with consideration to the mechanical behaviour of roof rock.

Despite the above successes in the study of mechanical characteristics, permeability performance, fracture propagation of the confining rock, and the fracture zone determination, the evolution law of fracture zone and its influence factors are still unclear. In addition, the amount of studies illustrated that the fracture zone around a UCG cavity is related to geological and operating conditions [5,29–34]. However, observation by Huang et al. [35], Zhang et al. [36], Wu and Jiang [37] through physical and numerical modelling suggests that the formation of a fracture zone that evolves during UCG is obviously different from that of coal mining. Additionally, quantitative description of the fracture zone distribution in coal mining is still a difficult task for the research community. A prediction model based on this aspect must depend on the empirical formulation with incomplete influence factors [38–40]. All of the above indicates that the existing mechanisms and models available are not proper for UCG cavities.

Therefore, in order to understand the evolution of fracture zones in the confining rock of a UCG cavity in terms of the mechanism and prediction model of the fracture zone, this paper implemented a series of numerical models associated with the thermal–mechanical coupling effect. The influencing factors of geological and operating conditions were taken into consideration, and the mechanism of fracture evolution and the fracture zone in terms

of the shear fracture and tensile fracture were analysed according to the numerical results. According to the characteristics of the evolution of fracture propagation, a prediction model was proposed. A comparison between the calculation results and the orthogonal test data verifies the good capacity of this prediction model. The study in this paper provides a new methodology for predicting the fracture zone of a UCG cavity and a safety assessment approach for further study.

2. Methodology

2.1. Numerical Model Set Up

The UCG cavity, as plotted in Figure 1a, is formed by coal combustion between the injection well and production well. According to the experiment of Daggupati et al. [41], combustion and air flow induced cavity expansion which occurred mainly around the injection well, resulting in a hemispherical shape. Such a shape was also observed by Xin et al. [42] as an irregular rectangle similar to a pear. Once the height of a cavity arrived at the top of coal seam, continuous expansion with an increasing R value occurred, as shown in Figure 1a. In order to simplify the analysis on the cavity expansion process, the cross section of this cavity expansion was constructed in a numerical model as introduced in the following subsection.

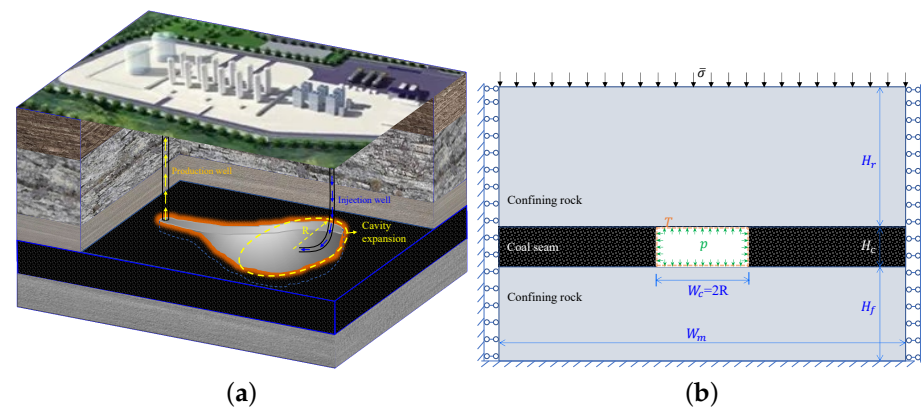


Figure 1. A cavity of underground coal gasification and the involved numerical model. (a) Prototype; (b) Numerical model.

The expanding cavity can be treated as an axisymmetric model, and according to the model used by Gao et al. [33], Perkins et al. [43], Khan et al. [44] for simplification, a 2D numerical model based on the vertical cross section along the R direction in Figure 1a is generalized. As displayed in Figure 1b, the bottom of this model is fixed and the boundaries of side walls are limited in normal displacement. An overburden pressure of $\bar{\sigma}$ is applied at the top boundary. Considering the gasification processes, the inner boundaries of the cavity are added with a gas pressure of P and temperature of T . The dimension of the cavity is defined as a rectangular area, which has a width of $W_c = 2R$ and a height of H_c equal to the thickness of the coal seam. The total width of this model is W_m , and a roof rock layer with a height of H_r and a base floor rock layer with a thickness of H_f are defined in this model. Detailed values of the above dimensions are defined in following subsections.

2.2. Influence Factor Recognition

From the perspective of the geological and operating conditions, the potential influence factors that control the fracture of confining rock during cavity expansion include the depth of the cavity, the mechanical properties of confining rock, the dimensions of the cavity, gasification pressure and temperature, etc. In order to quantify the factor levels, as listed in Table 1, the influence factors are graded by 5 levels. Specifically, considering that the direct roof of coal seam contains mud stone and sandstone, according to the Chinese standards for rock grade, the uniaxial compressive strength (UCS) ranged from 15 MPa

to 30 MPa, the average value of which is about 22.5 MPa. The average UCS of coal is approximately 10 MPa. Therefore, the UCS of graded rock is set as 16 MPa, 18 MPa, 20 MPa, 22 MPa, and 24 MPa corresponding to level I to level V, respectively, and the UCS of graded coal is defined as 6 MPa, 8 MPa, 10 MPa, 12 MPa, and 14 MPa corresponding to levels I to V, respectively. It is notable that the grade of coal and rock in Table 1 only represents the strength that controlling the stability of confining rock; therefore, plastic criterion must be involved. Mohr–Coulomb criterion was applied in the modelling, and according to the Mohr–Coulomb theory, the cohesion and friction angle of rock and coal are calculated according to the defined UCG of different levels. Detailed parameters are listed in Tables 2 and 3. The tension strength in Tables 2 and 3 are set at 1/15 of its UCS value according to the statistical result of Qi et al. [45]. Considering the deep conditions of UGS, the depth of cavity is defined with a range of 800 m to 1500 m. As shown in Table 1, for the dimension of a cavity, let its height equal to the thickness of coal seam; its width, as suggested by Jowkar et al. [46], is normally a multiple of its height in the context of well production; and the ratio of cavity width to its height is approximately 4 in the experiment. In our case, the ratio of cavity width to height is set to 2 to 6 times. According to the study of Pankiewicz-Sperka et al. [47] and Sadasivam et al. [48], the gasification pressure in the numerical modelling is set at 5 MPa to 9 MPa for different levels.

Table 1. Influence factors and their levels.

Factors	Level I	Level II	Level III	Level IV	Level V
F1: Grade of rock	1	2	3	4	5
F2: Depth of cavity (m)	800	975	1150	1325	1500
F3: Grade of coal	1	2	3	4	5
F4: Ratio of cavity width to height	2	3	4	5	6
F5: Thickness of coal seam (m)	5	10	15	20	25
F6: Gasification pressure (MPa)	5	6	7	8	9

Table 2. Mechanical properties of graded rock.

Parameters	Level I	Level II	Level III	Level IV	Level V
Cohesion C_r^o (MPa)	3.562	4.007	4.452	4.898	5.343
Friction angle ϕ_r^o (°)	42	42	42	42	42
Tension strength σ_{Tr}^o	1.067	1.2	1.333	1.467	1.6

Table 3. Mechanical properties of graded coal.

Parameters	Level I	Level II	Level III	Level IV	Level V
Cohesion C_c^o (MPa)	1.431	1.908	2.385	2.862	3.339
Friction angle ϕ_c^o (°)	39	39	39	39	39
Tension strength σ_{Tc}^o	0.533	0.667	0.8	0.933	1.067

As the temperature in the cavity is very high, the maximum of which will reach up to 1200 °C, therefore, the thermal damage of the confining rock is non-negligible. In order to account the thermal damage into the numerical model, the thermal-dependent mechanical parameters of coal were determined according to the laboratory test of Otto and Kempka [11], as plotted in Figure 2a, where the scatters are the experimental data and the curves are the fitted results. As a result, the plastic parameters of coal can be expressed as

$$C_c = C_c^o \left(0.016 + \frac{0.984}{1 + \left(\frac{T}{228} \right)^{12.8}} \right) \quad (1)$$

$$\phi_c = \phi_c^0 \left(0.015 + \frac{0.985}{1 + \left(\frac{T}{241} \right)^{10}} \right) \quad (2)$$

$$\sigma_{Tc} = \sigma_{Tc}^0 \left(0.19 + \frac{0.81}{1 + \left(\frac{T}{148} \right)^{4.4}} \right) \quad (3)$$

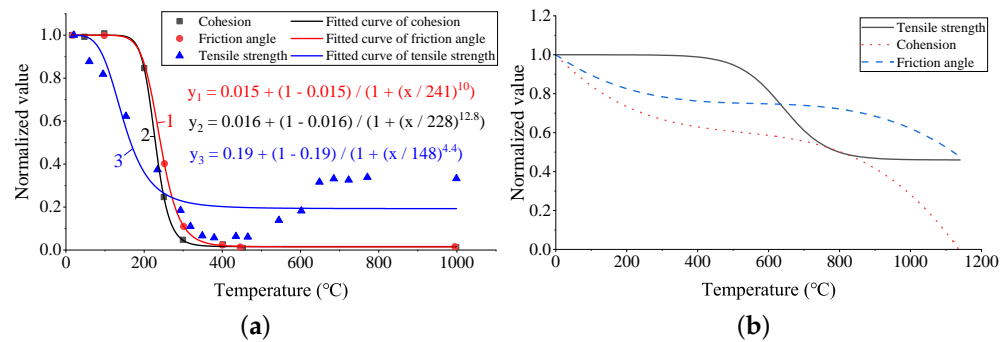


Figure 2. Mechanical parameters of coal and sandstone with variable temperature (after Otto and Kempka [11], Liu et al. [49]). (a) Coal; (b) Sandstone.

Since the thermal–mechanical performance of coal and rock are different, the variable parameters of coal and rock materials are set differently. The parameters of rock materials, as the referenced expression of Liu et al. [49] which is plotted in Figure 2b, are described by the detailed mathematical formulations

$$C_r = C_r^0 (1.025 - 0.0019T + 3.2668 \times 10^{-6}T^2 - 2.0851 \times 10^{-9}T^3) \quad (4)$$

$$\phi_r = \phi_r^0 (1.0013 - 0.00125T + 2.15 \times 10^{-6}T^2 - 1.2786 \times 10^{-9}T^3) \quad (5)$$

$$\sigma_{Tr} = \sigma_{Tr}^0 \left(0.4086 + \frac{0.5406}{1 + \exp\left(\frac{T-0.617}{62.6259}\right)} \right) \quad (6)$$

where C , ϕ , and σ_T are the cohesion, friction angle, and tensile strength, respectively, and the c and r subscripts represent coal and rock material.

For alternative thermal–mechanical parameters, referencing the parameters measured by Otto and Kempka [11], the elastic modulus, Poisson ratio, density, thermal conductivity, heat capacity, and linear thermal expansion coefficient of coal and sandstone were set as Table 4.

Table 4. Thermal–mechanical parameters of coal and sandstone.

Parameters	Unit	Coal	Sandstone
Elastic modulus	GPa	2	4
Poisson ratio	-	0.36	0.3
Density	kg/m ³	1360	2500
Thermal conductivity	W/m/K	0.23	2.3
Specific heat capacity	J/kg·K	2000	1363
Thermal expansion coefficient	K ⁻¹	5×10^{-6}	1.6×10^{-5}

As announced by Pavlo and Berdnyk [50], the velocity of the combustion of the working face is a key parameter to the stress–strain state of a rock mass. In this study, the

velocity of combustion was set at 0.6 m/day, as suggested by Perkins and Sahajwalla [51]. This velocity was realized by controlling the excavation steps in the numerical model.

3. Analysis of a Cavity Expansion

3.1. Procedure of a Cavity Expansion

In order to analyse the procedure of cavity expansion, ABAQUS software is applied in this study. ABAQUS is a well-known numerical software in thermal–mechanical coupling modelling, and it is conventionally used for calculating groups of model by input subscript. The expansion of a cavity with a height of 15 m was calculated, and the grades of rock and coal are level III, as illustrated in Table 1. The depth of the cavity is set as 1150 m, the gasification pressure is defined as 7 MPa, and the maximum width of the involved cavity is set as 90 m. The computational results are shown in Figure 3, in which Figure 3a–c are the broken area and Figure 3d–f are the Mises stress distributions at various cavity widths. Figure 3 plotted the typical changes in the characteristics of the fracture zone when the diameters of the cavity increased at 15 m, 40 m, and 90 m, respectively. The grey areas represent the shear failure zone, and the red areas denote the tensile fracture. In the subcaption, 2R is the width of a cavity expansion equivalent to that in Figure 1a.

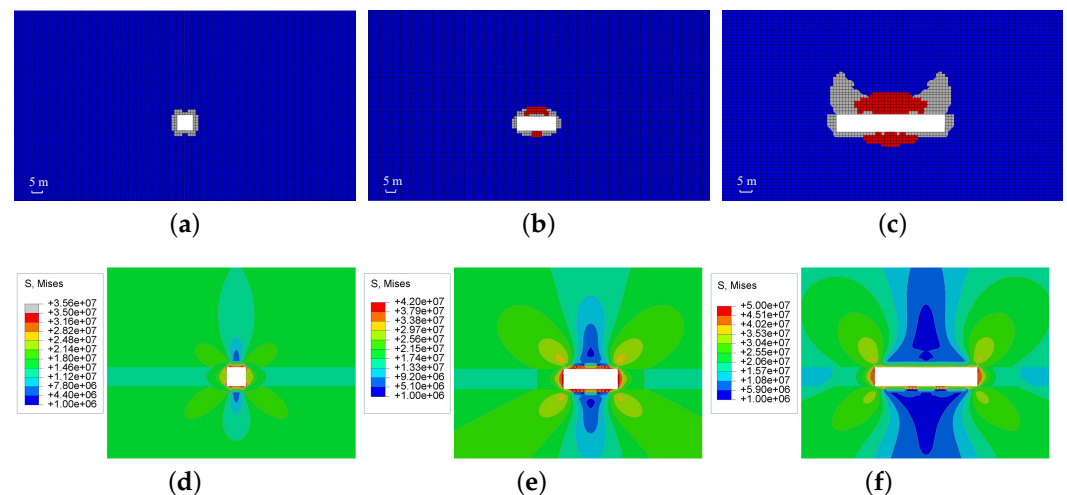


Figure 3. Numerical results of a cavity expansion. (a) Broken area (2R = 15 m); (b) Broken area (2R = 40 m); (c) Broken area (2R = 90 m); (d) Mises stress (2R = 15 m); (e) Mises stress (2R = 40 m); (f) Mises stress (2R = 90 m).

When the width of a cavity is 15 m, as plotted in Figure 3a, only shear failure occurred around the cavity due to the concentrated shear stress (see Figure 3d) at the near-field confining rock. Once the cavity expanded to 40 m, as displayed in Figure 3b, shear fracture still appeared around the cavity, while tensile fracture occurred at the roof and middle part of the base board. The Mises stress distribution (Figure 3e) denotes that deeper stress concentrated mainly at the side walls and the side area of roof layer. It is notable that, as shown in Figure 3c, the shear fracture height propagated quickly when the cavity expanded to 90 m. Figure 3f denotes the Mises stress mainly around the side corner and along the vertical direction. Simultaneously, tensile fracture area was enlarged at both the roof and base board.

As a whole, the expansion of the cavity experienced an initial near-field rock breakage due to shear fracture and roof and base board breakage due to tensile and shear fracture and shear fracture propagation along the vertical direction. The mechanism of these processes is analysed in the following subsection.

3.2. Mechanism of Confining Rock Broken and Risk Analysis

Corresponding to the procedure of Figure 3a–c, the mechanism of confining rock breakage can be demonstrated, as in Figure 4a–c. For a small-scale cavity, as shown in Figure 4a, despite the gasification pressure which supports part of the confining pressure, the thermal damage and local stress concentration creates a circle breakage zone. This condition is similar to the loose zone of a roadway [52,53]. With the increase in cavity width (Figure 4b), as described by Zhu et al. [54], Bai et al. [55], a caving arch is formed in the roof rock layer, while the fractured rock under this arch has the potential to fall. Successive expansion of the cavity, as demonstrated in Figure 4c, caused two ends of the carving arch to be broken, resulting in a simple supporting beam. Consequently, the shearing band propagated upwards, and the middle part of the supporting beam was fractured by tensile force. Additionally, the base board was fractured downwards due to the counter force from the underlying rock layers.

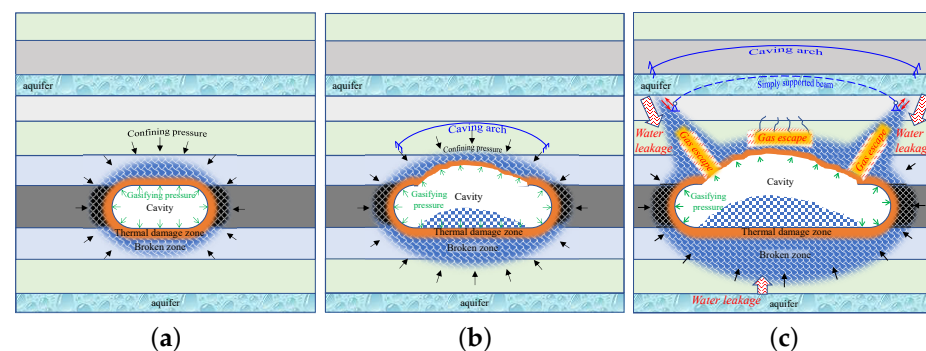


Figure 4. Mechanism of the confining rock breakage during cavity broken and potential risks. (a) Small-scale cavity; (b) Middle-scale cavity and (c) Large-scale cavity.

Coal combustion and water consumption are involved in UCG. For the safe operation of UCG, gas emissions are not allowed, due to environmental safety concerns [56], and water inrush is also limited to a restricted level to guarantee an efficient reaction in the cavity [57]. However, in the case of Figure 4c, progressive propagation of the rock fracture in roof layers of a cavity induces not only gas emission to the water aquifer but also water inrush into the UCG chamber. If the water aquifer existed underlying the UCG cavity, a broken base board has the potential to lead to water inrush under the hydraulic pressure. Therefore, the height of the fracture in the roof rock layers and the depth of the fracture propagated in the base board are the key indices of safety assessment of a UCG cavity.

3.3. Thermal Damage Analysis

After a cavity was formed, the temperature distribution in the confining rock is displayed in Figure 5. Obviously, temperature decreased dramatically away from the inner face of a cavity. Specifically, the temperature at the inner face of a cavity is 1200 °C, which was decreased to about 500 °C at a depth of approximately 2 m and around 200 °C at a depth of about 3.5 m. This result is close to the data obtained by Xin et al. [58], Kapusta [59]. Figure 2 suggests that the mechanical performance of coal and sandstone have a small change below the temperatures of 200 °C and 500 °C, respectively. Therefore, it is reasonable to say temperature has limited influence on the thermal damage in the confining rock of a cavity, exhibiting a maximum depth of 3.5 m.

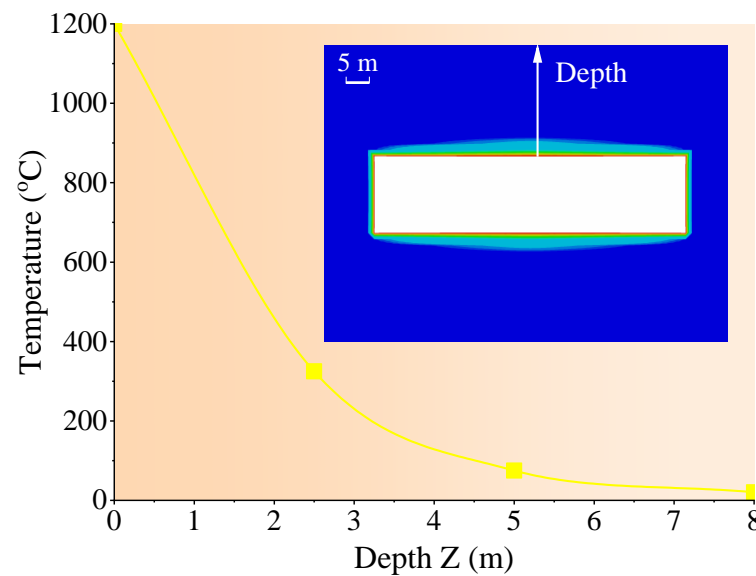


Figure 5. Distribution of temperature in confining rock.

4. Evolution of Fracture Zone

The evolution of the fracture zone in the roof layers and the base board of the cavity are calculated with variable influence factors. Figure 6a–f is the calculated fracture height in the roof layers and base board with variable levels of rock grade, overburden pressure, grade of coal seam, ratio of cavity width to height, thickness of coal seam, and gasification pressure, respectively.

As plotted in Figure 6, the fracture in the roof layers change obviously with different influence factors, resulting in shear fracture, tensile fracture, or contrast. Specifically, the higher grade (harder) decreases the height of shear fracture (Figure 6), while the tensile fracture in the roof has a limited change. Once the height of the shear fracture is smaller than that of the tensile fracture, the pattern of the confining fracture is changed from a simply supported beam to a caving arch, as mentioned in Figure 4b,c. Such phenomenon can also be seen in Figure 6f. The higher gasification pressure is able to decrease the shear fracture and lead to a change in pattern. To the contrary, as displayed in Figure 6b,d,e, the promoted overburden pressure, ratio of cavity width to height, and the thickness of coal seam increase the shear fracture height, thereby changing the broken pattern from a caving arch to a simply supported beam. Interestingly, as shown in Figure 6c, the grade of coal seam has almost no influence on the height of fracture in both the roof layers and base board. Obviously, the fracture depth in the base board is mainly induced by tensile fracture, and the fractures in the coal seam are small relative to those in the roof and base board.

Additionally, Figure 6 shows a limitation of minimal fracture height or depth in both shear fracture and tensile fracture, which ranges from about 3.5 m to 5 m. As demonstrated in Figure 5, such a limitation is mainly due to the thermal damage.

It is notable that, as demonstrated in Figure 4c, both the shear fracture and tensile fracture compose the channel of fluid conductivity into a cavity. Therefore, despite the pattern change during the cavity expansion with different factors, the outline of the fracture dimensions in Figure 6 should be treated as the available depth of water conductivity and gas emission.

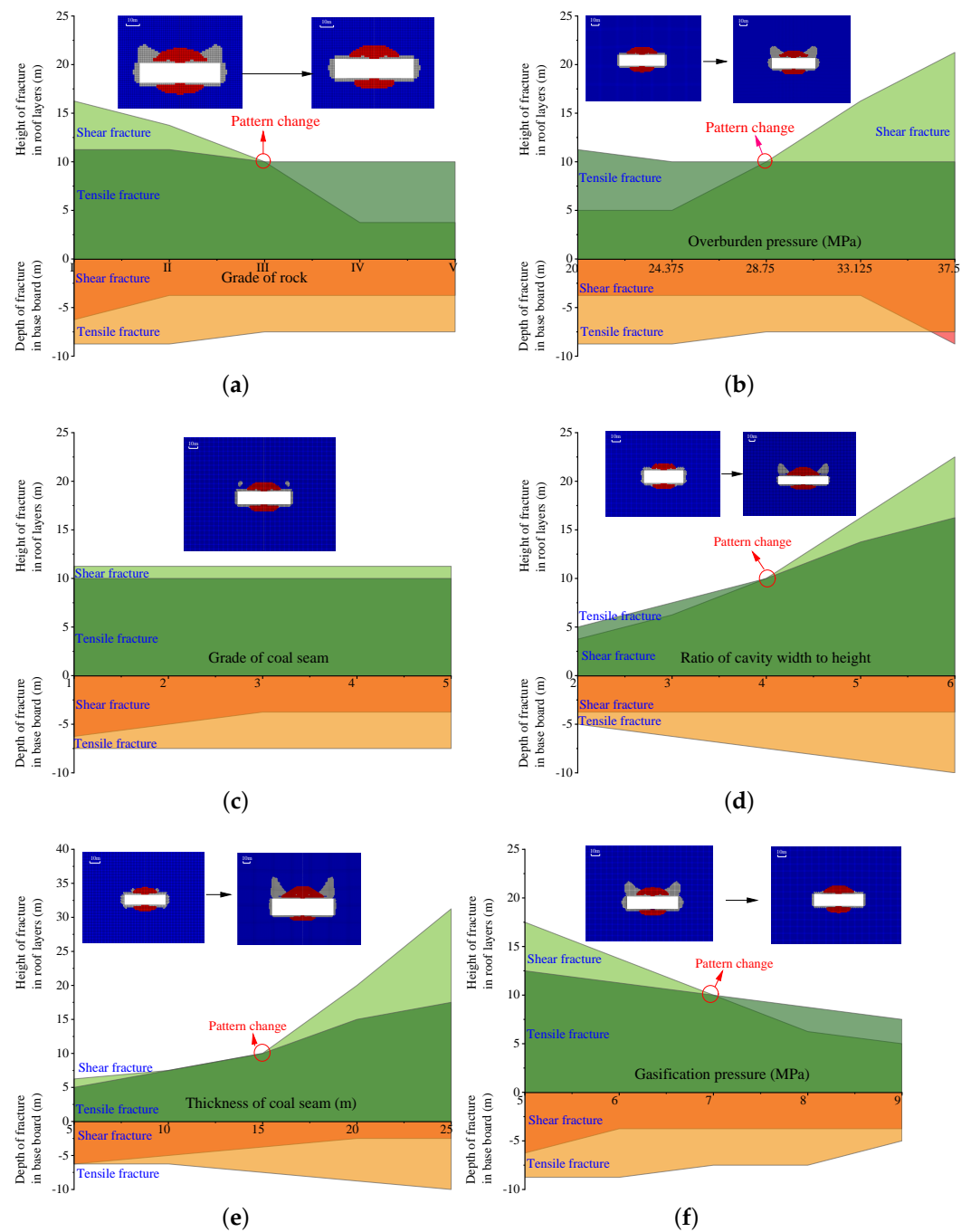


Figure 6. Evolution of fracture height with variable levels in (a–f) grade of rock, overburden pressure, grade of coal seam, ratio of cavity width to height, thickness of coal seam, and gasification pressure, respectively.

5. A Model for Fracture Height and Depth

5.1. Model Setup

The above analysis on the evolution of the fracture zone with variable levels of influence factors suggests that both the shear fracture and tensile fracture induced by different factors have a nearly linear relationship with various levels to some extent, and the amount of total fracture height or depth of the fluid channel has the potential to cause a change in pattern. On account of these characteristics, the height and depth of fracture can be determined, as illustrated in Figure 7. Specifically, for the decreasing tendency (see Figure 7a) corresponding to the tendencies in Figure 6a,f, the outline of fracture height

(H) in the roof can be determined by the maximum value of height of the tensile and shear fracture (h_1 and h_2), and the limitation of thermal damage thickness, namely $H > h_t$. Similarly, the depth of fracture (D) is also constrained by the maximum value of the shear and tensile fractures ($|d_1|$ and $|d_2|$) and thermal damage thickness (means $D < d_t$). For the increasing tendency, which represents the conditions of Figure 6b,d,e, the total fracture height or depth for the fluid channel can also be obtained according to the constraints of the maximum of the tensile and shear fractures and the thermal damage thickness. In the light of the method denoted in Figure 7, the model for predicting the height and depth of fluid channel can be established as follows:

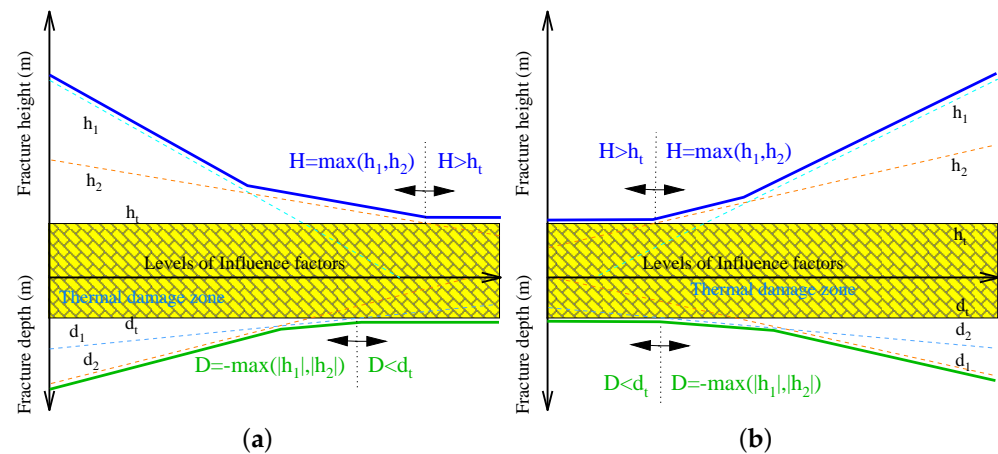


Figure 7. Sketch for determination of the total height and depth of fracture. (a) Decreasing tendency; (b) Increasing tendency.

Firstly, the linear relationship of fracture height and depth to the influence factor levels can be defined as

$$\begin{cases} h_1 = \alpha_1 x + \beta_1 \\ h_2 = \alpha_2 x + \beta_2 \\ d_1 = \gamma_1 x + \delta_1 \\ d_2 = \gamma_2 x + \delta_2 \end{cases} \quad (7)$$

where α_1 , α_2 , γ_1 and γ_2 are the slopes and β_1 , β_2 , δ_1 , and δ_2 are the intercepts. Then, in light of the outline as demonstrated in Figure 7, the fracture height in the roof and that in the base board are expressed as

$$\begin{cases} H = \max(h_1, h_2) & (H > h_t) \\ H = h_t & (H \leq h_t) \end{cases} \quad (8)$$

$$\begin{cases} D = \max(d_1, d_2) & (D > d_t) \\ D = d_t & (D \leq d_t) \end{cases} \quad (9)$$

As the linear relationship of Equation (7) can be developed according to the chain rule, for all the levels of influence factors, Equation (7) can be developed as

$$\begin{cases} h_1 = \sum_{i=1}^n \alpha_i^1 X_i + \beta_1 \\ h_2 = \sum_{i=1}^n \alpha_i^2 X_i + \beta_2 \\ d_1 = \sum_{i=1}^n \gamma_i^1 X_i + \delta_1 \\ d_2 = \sum_{i=1}^n \gamma_i^2 X_i + \delta_2 \end{cases} \quad (10)$$

in which X_i is the level of i -th influence factor. Combining Equation (8) with Equation (10), the total fracture height and depth for the fluid channel in the roof and base board of a cavity can be finally predicted.

According to the theory of multiple linear regression, as listed in Table 5, the coefficients in Equation (10) can be determined associated with the data in Figure 6. The variables X_1 to X_5 denote the grade of rock, overburden pressure, ratio of cavity width to height, thickness of coal seam, and gasification pressure, respectively. For the grade of coal seam, which is omitted due to the nearly negligible influence by which on the fracture height and depth, the residual squares of such regressions ranged from about 0.839 to 0.975 (please see Table 5), especially for the height of the shear and tensile fractures, which are close to 1, indicating the high accuracy of the proposed model. The residual square of the fracture depth is lower than 0.9, this is because of fluctuation in data as plotted in Figure 6. Despite such relatively large errors, the accuracy of such regression results are still acceptable for the small value of fracture depth.

Table 5. Coefficients determined by multiple linear regression.

Levels of Influence Factors	α_1	α_2	γ_1	γ_1
X_1	−3.579	−0.284	2.046	0.198
X_2	1.482	−0.05	−0.683	0.086
X_3	5.38	2.875	0	−1.25
X_4	1.937	0.65	0.08	−0.2
X_5	−3.296	−1.25	1.28	0.875
Intercepts	β_1	β_2	δ_1	δ_2
Value	−34.96	0.315	−5.665	−8.83
Residual square	0.975	0.974	0.839	0.874

5.2. Model Validation

In order to validate the prediction model, an orthogonal test was conducted by numerical modelling, and the numerical model and parameters used are the same as in Figure 1b and Tables 2 and 3. The orthogonal test was designed with six factors, and each factor has five levels. According to the theory of the orthogonal test, 25 cases were calculated. The test cases and results are listed in Table 6. The alpha H and D in Table 6 represent the height of the fracture zone in the roof rock and the depth of the fracture in the base board, respectively. Obviously, the fracture height in Table 6 ranged from 2.5 m to 53.75 m, which is larger than the fracture depth. Applying Equation (8) to Equation (10) and the coefficients in Table 5, the predicted data and numerical results are compared in Figure 8.

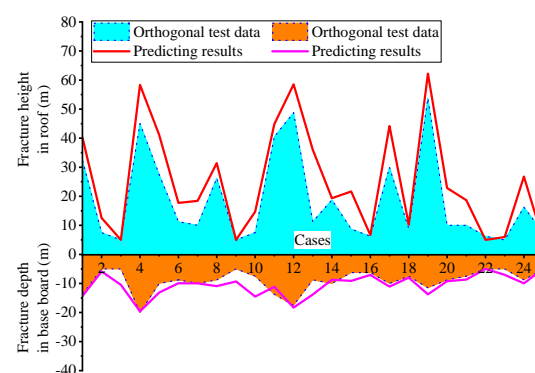


Figure 8. Comparison of the orthogonal test and prediction results.

Table 6. Cases for orthogonal test and calculated results.

Cases	F1	F2	F3	F4	F5	F6	H (m)	D (m)
1	1	1150	2	5	15	6	32.5	−13.75
2	5	1150	5	2	25	8	7.5	−5
3	1	800	1	2	5	5	2.5	−5
4	2	1500	5	6	15	5	45	−20
5	1	1325	5	4	20	9	27.5	−10
6	4	1150	3	4	10	5	11.25	−8.75
7	5	1325	3	6	5	6	10	−10
8	4	800	2	6	25	9	26.25	−8.75
9	2	1150	4	3	5	9	5	−5
10	3	1500	2	4	5	8	7.5	−7.5
11	3	1150	1	6	20	7	40.5	−13.75
12	1	1500	3	3	25	7	48.75	−17.5
13	4	1500	4	2	20	6	11.25	−8.75
14	5	1500	1	5	10	9	18.75	−10
15	5	975	2	3	20	5	8.75	−6.25
16	4	975	5	5	5	7	6.25	−6.25
17	2	975	1	4	25	6	30	−10
18	5	800	4	4	15	7	8.75	−7.5
19	3	1325	4	5	25	5	53.75	−11.5
20	1	800	4	6	10	8	10	−8.75
21	4	1325	1	3	15	8	10	−7.5
22	3	975	3	2	15	9	6.25	−5
23	3	800	5	3	10	6	5	−5
24	2	800	3	5	20	8	16.25	−8.75
25	2	1325	2	2	10	7	7.5	−5

Obviously, Figure 8 suggests that both the predicting results for fracture height and depth have a similar tendency to that of the orthogonal test results. The prediction results in Figure 8 are relatively higher than the data from orthogonal test in the fracture height in the roof and those of the fracture depth in the base board are close to each other. Despite the difference between the orthogonal data and prediction data, the prediction results covered all the orthogonal results, which means that estimation based on the prediction data for the fluid channel is safer.

As a whole, the predicting data in Figure 8 match well with the orthogonal data to some extent, especially the peak value to the fluctuating curves, which convince us that the prediction model is capable of estimating the fracture height in the roof and that of the depth in the base board for a UCG cavity.

6. Conclusions

This paper targets fracture evolution in the confining rock during UCG cavity expansion. According to the expansion process of a cavity, a numerical model considering different factors in terms of geological and operating conditions was implemented for analysis on the cavity expansion and fracture zone evolution. This paper clarified the mechanism of fracture propagation during a UCG cavity, distinguished the influence factors on the fracture propagation, and proposed a prediction model for the fracture height and depth in roof and baseboard, respectively. Conclusions of this paper can be remarked as:

- (i) With the expansion of a UCG cavity, the near-field rock is initially broken. Then, a caving arch is formed due to cracks in the roof rock. Subsequently, shear fracture propagated upward due to the failure of caving arch at two springers.
- (ii) The grade of confining rock, depth, dimension of the cavity, and gasifying pressure are the controlling factors in the fracture evolution, especially the fracture height in roof layers.

- (iii) Comparison of the orthogonal test and prediction results suggests that the proposed model has a good ability to estimate the fracture zone for the assessment of safety of the UCG cavity.

This paper provides an approach to the prediction of fracturing distribution, not only in the fracture pattern, but also the height and depth in both roof and baseboard, which is the basis for safety assessment of environmental risks and site selection. Therefore, further study should be concentrated at the field verification of the proposed mechanism and model and the methodology of the safety evaluation of water leakage or gas emission through the fracture zone according to the mechanism and model.

Author Contributions: Conceptualization, Z.D. and Y.Z.; methodology, H.Y.; software, H.Y.; validation, X.W., T.C. and J.X.; formal analysis, H.W.; investigation, H.Y. and S.C.; resources, Z.D., X.W. and H.W.; data curation, M.Z.; writing—original draft preparation, H.Y. and Y.Z.; writing—review and editing, H.Y. and T.C.; visualization, M.Z. and H.C.; project administration, Z.D.; funding acquisition, Z.D., H.Y. and T.C. All authors have read and agreed to the published version of the manuscript.

Funding: This paper is funded by the Major Scientific and Technological Project of China National Petroleum Corporation (CNPC) (Grant No. 2019E-25), the National Natural Science Foundation of China (Grant No. 52004090 and 52274199), and the project of National Science Foundation of Hebei Province (Grant No. E2020508025).

Institutional Review Board Statement: Not applicable.

Informed Consent Statement: Not applicable.

Data Availability Statement: The data for this study is included in this paper.

Conflicts of Interest: The authors declare no conflict of interest.

References

1. Bhutto, A.W.; Bazmi, A.A.; Zahedi, G. Underground coal gasification: From fundamentals to applications. *Prog. Energy Combust. Sci.* **2013**, *39*, 189–214. [\[CrossRef\]](#)
2. McInnis, J.; Singh, S.; Huq, I. Mitigation and adaptation strategies for global change via the implementation of underground coal gasification. *Mitig. Adapt. Strateg. Glob. Chang.* **2016**, *21*, 479–486. [\[CrossRef\]](#)
3. Kaveh, N.S.; Barnhoorn, A.; Wolf, K. Investigation on Mechanical Behaviour of Coal and Overburden Rock for UCG. In Proceedings of the 77th EAGE Conference and Exhibition 2015. European Association of Geoscientists & Engineers, Madrid, Spain, 1–4 July 2015; Volume 2015, pp. 1–5.
4. Ding, Q.L.; Ju, F.; Song, S.B.; Yu, B.Y.; Ma, D. An experimental study of fractured sandstone permeability after high-temperature treatment under different confining pressures. *J. Nat. Gas Sci. Eng.* **2016**, *34*, 55–63. [\[CrossRef\]](#)
5. Meng, T.; Guangwu, X.; Jiwei, M.; Yang, Y.; Liu, W.; Zhang, J.; Bosen, J.; Fang, S.; Ren, G. Mixed mode fracture tests and inversion of FPZ at crack tip of overlying strata in underground coal gasification combustion cavity under real-time high temperature condition. *Eng. Fract. Mech.* **2020**, *239*, 107298. [\[CrossRef\]](#)
6. Wiatowski, M.; Stańczyk, K.; Świądrowski, J.; Kapusta, K.; Cybulski, K.; Krause, E.; Grabowski, J.; Rogut, J.; Howaniec, N.; Smoliński, A. Semi-technical underground coal gasification (UCG) using the shaft method in Experimental Mine “Barbara”. *Fuel* **2012**, *99*, 170–179. [\[CrossRef\]](#)
7. Orlov, G. The effects of rock deformation in underground coal gasification. In *Underground Coal Gasification and Combustion*; Elsevier: Amsterdam, The Netherlands, 2018; pp. 283–327.
8. Luo, J.; Wang, L. High-temperature mechanical properties of mudstone in the process of underground coal gasification. *Rock Mech. Rock Eng.* **2011**, *44*, 749–754. [\[CrossRef\]](#)
9. Akbarzadeh, H.; Chalaturnyk, R.J. Structural changes in coal at elevated temperature pertinent to underground coal gasification: A review. *Int. J. Coal Geol.* **2014**, *131*, 126–146. [\[CrossRef\]](#)
10. Janoszek, T.; Łączny, M.J.; Stańczyk, K.; Smoliński, A.; Wiatowski, M. Modelling of gas flow in the underground coal gasification process and its interactions with the rock environment. *J. Sustain. Min.* **2013**, *12*, 8–20. [\[CrossRef\]](#)
11. Otto, C.; Kempka, T. Thermo-mechanical simulations of rock behavior in underground coal gasification show negligible impact of temperature-dependent parameters on permeability changes. *Energies* **2015**, *8*, 5800–5827. [\[CrossRef\]](#)
12. Wałowski, G. Gas permeability model for porous materials from underground coal gasification technology. *Energies* **2021**, *14*, 4462. [\[CrossRef\]](#)
13. Madiutomo, N.; Hermawan, W.; Pamungkas, M. The effect of rock permeability value on groundwater influx in underground coal gasification reactor. *Proc. IOP Conf. Ser. Earth Environ. Sci.* **2021**, *882*, 012054. [\[CrossRef\]](#)

14. Ding, K.; Wang, L.; Ren, B.; Li, Z.; Wang, S.; Jiang, C. Experimental study on relative permeability characteristics for CO₂ in sandstone under high temperature and overburden pressure. *Minerals* **2021**, *11*, 956. [\[CrossRef\]](#)
15. Duan, T.H.; Zhang, J.M.; Mallett, C.; Li, H.H.; Huo, L.W.; Zhao, K.T. Numerical simulation of coupled thermal-mechanical fracturing in underground coal gasification. *Proc. Inst. Mech. Eng. Part A J. Power Energy* **2018**, *232*, 74–84. [\[CrossRef\]](#)
16. Jin, P.; Hu, Y.; Shao, J.; Liu, Z.; Feng, G.; Song, S. Influence of temperature on the structure of pore–fracture of sandstone. *Rock Mech. Rock Eng.* **2020**, *53*, 1–12. [\[CrossRef\]](#)
17. Zheng, H.H.; Zhang, X.H.; Liu, X.L.; Chen, L.J. Numerical Simulation of Stress Field of Surrounding Strata in Underground Gasification of Coal. *Coal Min. Technol.* **2011**, *16*, 17–19.
18. Li, C.; Xin, L.; Xu, M.; Li, J.; Han, L.; An, M. Study of thermal-mechanical coupling numerical simulation of similar simulation experiment of underground coal gasification. *Coal Sci. Technol.* **2019**, *47*, 226–233.
19. Škvareková, E.; Tomašková, M.; Wittenberger, G.; Zelenák, Š. Analysis of risk factors for underground coal gasification. *Manag. Syst. Prod. Eng.* **2019**, *4*, 227–235. [\[CrossRef\]](#)
20. Thomas, H.; Hosking, L.; Sandford, R.; Zagorščak, R.; Chen, M.; An, N. Deep ground and energy: Carbon sequestration and coal gasification. *Proc. Int. Congr. Environ. Geotech.* **2018**, *1*, 38–60.
21. Roullier, B.; Langston, P.; Li, X. Modelling the environmental impact of underground coal gasification. In *Energy Geotechnics*; Springer: Cham, Switzerland, 2016; pp. 335–342.
22. Jia, B.; Chen, Z.; Xian, C. Investigations of CO₂ storage capacity and flow behavior in shale formation. *J. Pet. Sci. Eng.* **2022**, *208*, 109659. [\[CrossRef\]](#)
23. Li, Z.; Wang, L.; Ren, B.; Ding, K. The Layout of the Combustion Cavity and the Fracture Evolution of the Overlying Rock during the Process of Underground Coal Gasification. *Geofluids* **2022**, *2022*, 9264959. [\[CrossRef\]](#)
24. Qin, S. Study on Development Law of Water Diversion Fracture Zone of Underground Coal Gasification. Master's Thesis, China University of Mining and Technology, Xuzhou, China, 2018.
25. Lu, Y.L.; Wang, L.G.; Tang, F.R.; He, Y. Fracture evolution of overlying strata over combustion cavity under thermal mechanical interaction during underground coal gasification. *J. China Coal Soc.* **2012**, *37*, 1292–1298.
26. Lin, G. Numerical Analysis of the Development of Induced Water Fractured Zone and Groundwater Seepage Field in Underground Coal Gasification. Ph.D. Thesis, China University of Mining and Technology, Xuzhou, China, 2016.
27. Liu, J. Study on the Combustion Cavity Growth and Stability of the Roof during Underground Coal Gasification. Master's Thesis, China University of Mining and Technology, Xuzhou, China, 2014.
28. Falshtynskyi, V.; Lozynskyi, V.; Saik, P.; Dychkovskyi, R.; Tabachenko, M. Substantiating parameters of stratification cavities formation in the roof rocks during underground coal gasification. *Min. Miner. Depos.* **2016**, *10*, 16–24. [\[CrossRef\]](#)
29. Su, F.q.; Hamanaka, A.; Itakura, K.i.; Zhang, W.; Deguchi, G.; Sato, K.; Takahashi, K.; Kodama, J.I. Monitoring and evaluation of simulated underground coal gasification in an ex-situ experimental artificial coal seam system. *Appl. Energy* **2018**, *223*, 82–92. [\[CrossRef\]](#)
30. Xie, J.; Xin, L.; Hu, X.; Cheng, W.; Liu, W.; Wang, Z. Technical application of safety and cleaner production technology by underground coal gasification in China. *J. Clean. Prod.* **2020**, *250*, 119487. [\[CrossRef\]](#)
31. Feng, M.; Xin, L.; Li, K.; Wu, J.; Li, J.; Cheng, W.; Wang, B. Discussion on requirements of gasifier gas tightness for underground coal gasification production. *Sustain. Energy Technol. Assess.* **2021**, *47*, 101550. [\[CrossRef\]](#)
32. Shahbazi, M.; Najafi, M.; Fatehi Marji, M.; Abdollahipour, A. Cavity Growth in Underground Coal Gasification Method by Considering Cleat Length and Inclination of Coal with Elasto-Brittle Behavior. *J. Min. Environ.* **2022**, *13*, 607–625.
33. Gao, W.; Zagorščak, R.; Thomas, H.R. Insights into solid-gas conversion and cavity growth during Underground Coal Gasification (UCG) through Thermo-Hydraulic-Chemical (THC) modelling. *Int. J. Coal Geol.* **2021**, *237*, 103711. [\[CrossRef\]](#)
34. Itakura, K.; Wakamatsu, M.; Sato, M.; Goto, T.; Yoshida, Y.; Ohta, M.; Shimada, K.; Belov, A.; Ram, G. Fundamental experiments for developing underground coal gasification (UCG) system. *Mem. Muroran Inst. Technol.* **2010**, *59*, 51–54.
35. Huang, W.; Wang, Z.; WU, S.; Huo, L.; Zhang, X.; Yan, R. Determining Method for Length of the Shortwall Face with Thermal-Mechanical Coupling Effects of Underground Coal Gasification. *J. Taiyuan Univ. Technol.* **2019**, *2*, 153–159.
36. Zhang, H.; Zhao, K.; Wang, L.; Yan, H. On the migrating regularity of the overlying strata in the combustible space area in the underground coal gasification. *J. Saf. Environ.* **2016**, *6*, 89–92.
37. Wu, C.; Jiang, X. Research progress of temperature field and heat transfer characteristics in process of underground coal gasification. *Coal Sci. Technol.* **2022**, *1*, 275–285.
38. Majdi, A.; Hassani, F.; Nasiri, M. Prediction of the height of destressed zone above the mined panel roof in longwall coal mining. *Int. J. Coal Geol.* **2012**, *98*, 62–72. [\[CrossRef\]](#)
39. Dai, S.; Han, B.; Liu, S.; Li, N.; Geng, F.; Hou, X. Neural network-based prediction methods for height of water-flowing fractured zone caused by underground coal mining. *Arab. J. Geosci.* **2020**, *13*, 495. [\[CrossRef\]](#)
40. Palchik, V. Analysis of main factors influencing the apertures of mining-induced horizontal fractures at longwall coal mining. *Geomech. Geophys.-Geo-Energy-Geo-Resour.* **2020**, *6*, 37. [\[CrossRef\]](#)
41. Daggupati, S.; Mandapati, R.N.; Mahajani, S.M.; Ganesh, A.; Mathur, D.; Sharma, R.; Aghalayam, P. Laboratory studies on combustion cavity growth in lignite coal blocks in the context of underground coal gasification. *Energy* **2010**, *35*, 2374–2386. [\[CrossRef\]](#)

42. Xin, L.; Li, J.; Xie, J.; Li, C.; Han, L.; An, M.; Xu, M.; Wang, Z. Simulation of cavity extension formation in the early ignition stage based on a coal block gasification experiment. *J. Energy Resour. Technol.* **2020**, *142*, 062304. [[CrossRef](#)]
43. Perkins, G.; Saghafi, A.; Sahajwalla, V. Numerical modeling of underground coal gasification and its application to Australian coal seam conditions. In Proceedings of the 18th Annual International Pittsburgh Coal Conference, Pittsburgh, PA, USA, 15–19 September 2003; Volume 18, pp. 1–12.
44. Khan, M.M.; Mmbaga, J.P.; Shirazi, A.S.; Liu, Q.; Gupta, R. Modelling underground coal gasification—A review. *Energies* **2015**, *8*, 12603–12668. [[CrossRef](#)]
45. Qi, L.; Yang, K.; Lu, W.; Yan, S. Statistical analysis on uniaxial compressive strength of coal measures. *Coal Sci. Technol.* **2013**, *41*, 100–103.
46. Jowkar, A.; Sereshki, F.; Najafi, M. A new model for evaluation of cavity shape and volume during Underground Coal Gasification process. *Energy* **2018**, *148*, 756–765. [[CrossRef](#)]
47. Pankiewicz-Sperka, M.; Kapusta, K.; Basa, W.; Stolecka, K. Characteristics of Water Contaminants from Underground Coal Gasification (UCG) Process—Effect of Coal Properties and Gasification Pressure. *Energies* **2021**, *14*, 6533. [[CrossRef](#)]
48. Sadasivam, S.; Zagorščak, R.; Thomas, H.R.; Kapusta, K.; Stańczyk, K. Experimental study of methane-oriented gasification of semi-anthracite and bituminous coals using oxygen and steam in the context of underground coal gasification (UCG): Effects of pressure, temperature, gasification reactant supply rates and coal rank. *Fuel* **2020**, *268*, 117330. [[CrossRef](#)]
49. Liu, X.; Guo, G.; Li, H. Thermo-mechanical coupling numerical simulation method under high temperature heterogeneous rock and application in underground coal gasification. *Energy Explor. Exploit.* **2020**, *38*, 1118–1139. [[CrossRef](#)]
50. Pavlo, S.; Berdnyk, M. Mathematical model and methods for solving heat-transfer problem during underground coal gasification. *Min. Miner. Depos.* **2022**, *16*, 87–94.
51. Perkins, G.; Sahajwalla, V. A mathematical model for the chemical reaction of a semi-infinite block of coal in underground coal gasification. *Energy Fuels* **2005**, *19*, 1679–1692. [[CrossRef](#)]
52. Tian, M.; Han, L.; Meng, Q.; Jin, Y.; Meng, L. In situ investigation of the excavation-loose zone in surrounding rocks from mining complex coal seams. *J. Appl. Geophys.* **2019**, *168*, 90–100. [[CrossRef](#)]
53. Lei, G.; Wang, G.; Luo, J.; Hua, F.; Gong, X. Theoretical Study of Surrounding Rock Loose Zone Scope Based on Stress Transfer and Work–Energy Relationship Theory. *Appl. Sci.* **2022**, *12*, 7292. [[CrossRef](#)]
54. Zhu, D.; Wu, Y.; Liu, Z.; Dong, X.; Yu, J. Failure mechanism and safety control strategy for laminated roof of wide-span roadway. *Eng. Fail. Anal.* **2020**, *111*, 104489. [[CrossRef](#)]
55. Bai, Q.S.; Tu, S.H.; Zhang, C.; Zhu, D. Discrete element modeling of progressive failure in a wide coal roadway from water-rich roofs. *Int. J. Coal Geol.* **2016**, *167*, 215–229. [[CrossRef](#)]
56. Imran, M.; Kumar, D.; Kumar, N.; Qayyum, A.; Saeed, A.; Bhatti, M.S. Environmental concerns of underground coal gasification. *Renew. Sustain. Energy Rev.* **2014**, *31*, 600–610. [[CrossRef](#)]
57. Mohanty, D. An overview of the geological controls in underground coal gasification. *Proc. IOP Conf. Ser. Earth Environ. Sci.* **2017**, *76*, 012010. [[CrossRef](#)]
58. Xin, L.; Cheng, W.; Xie, J.; Liu, W.; Xu, M. Theoretical research on heat transfer law during underground coal gasification channel extension process. *Int. J. Heat Mass Transf.* **2019**, *142*, 118409. [[CrossRef](#)]
59. Kapusta, K. Effect of lignite properties on its suitability for the implementation of underground coal gasification (UCG) in selected deposits. *Energies* **2021**, *14*, 5816. [[CrossRef](#)]